J. Fluid Mech. (2005), *vol.* 541, *pp.* 399–408.
doi:10.1017/S0022112005006269 Printed in the United Kingdom

Thermocapillary control of rupture in thin viscous fluid sheets

By B. S. TILLEY[1] AND M. BOWEN[2]†

[1]Franklin W. Olin College of Engineering, Olin Way, Needham, MA 02492, USA
[2]School of Mathematical Sciences, University of Nottingham, Nottingham, NG7 2RD, UK

(Received 24 March 2005 and in revised form 13 July 2005)

We consider the evolution of a thin viscous fluid sheet subject to thermocapillary effects. Using a lubrication approximation we find, for symmetric interfacial deflections, coupled evolution equations for the interfacial profile, the streamwise component of the fluid velocity and the temperature variation along the surface. Initial temperature profiles change the initial flow field through Marangoni-induced shear stresses. These changes then lead to preferred conditions for rupture prescribed by the initial temperature distribution. We show that the time to rupture may be minimized by varying the phase difference between the initial velocity profile and the initial temperature profile. For sufficiently large temperature differences, the phase difference between the initial velocity and temperature profiles determines the rupture location.

1. Introduction

In recent years, ink-jet printers have become a common and economical standard for producing high-quality printed text and graphics. These printers typically employ several different jets simultaneously, each made up of a different colour of ink; arbitrary colours can therefore be generated by mixing the output of the jets in different proportions. Since only one drop size is typically generated, the efficient control of drop formation is an inherent requirement in the overall performance of the system. The limitation on resolution of these devices depends on the reliable control of the smallest drop size while the printing rate depends on the ability to control the breakup phenomena both spatially and in time. A further application requiring the delicate control of jet dynamics is the fabrication of high-density microelectronic devices (Hayes, Wallace & Cox 1999; Molesa *et al.* 2003).

Herein, we consider the viability of using thermocapillary stresses to control both droplet size and breakup. Thermocapillary forces have been previously employed in a wide variety of applications. For example, Schatz & Neitzel (2001) reviewed experimental investigations of problems with axial temperature gradients in liquid bridges, and driven thermocapillary waves in slots. Temperature profiles have also been used in the investigation of thermocapillary-induced non-wetting (see Sumner, Wood & Neitzel 2003), the fingering instability found in thin films coating a substrate (see Garnier, Grigoriev & Schatz 2003) and the manipulation of drops within a viscous fluid (see Rybalko, Magome & Yoshikawa 2004).

† Present Address: Graduate School of Mathematical Sciences, University of Tokyo, Komaba, Tokyo 153-8914, Japan.

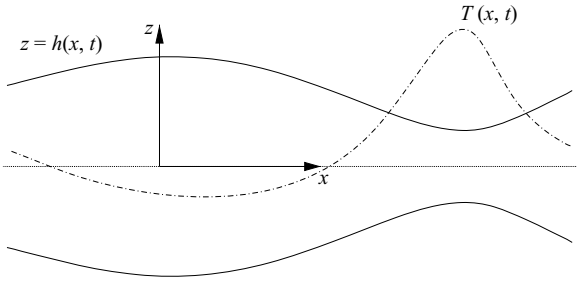

FIGURE 1. Schematic of the problem under consideration.

Since the characteristic thickness of the jets is typically around 10 μm, if a 1 mW laser pulse is applied for 1 ms along a section of the jet (say 1 mm in length), then the local temperature is increased by approximately 0.25 K. Although this is a small temperature difference, the resulting induced shear stress is strong enough to alter any initial inertial effects, and hence the fluid dynamics within the jet. Furthermore, the experimental investigation of Nahas & Panton (1990) found that the symmetrical heating of a larger water jet (of 2 mm radius) using a modulated laser can delay the onset of the classical Rayleigh instability. Consequently, controlling the rupture process for a thin jet by this mechanism is experimentally justifiable.

To focus on the competition between the thermally driven and inertially driven instability mechanisms, we consider a symmetrically heated sheet (rather than a radially symmetric jet), which results in no net bending. The application of the laser results in a prescribed initial temperature profile from which the sheet evolves. The spatial location of rupture is controlled through interfacial temperature gradients. We find that this heating, along with a standard modulation in the axial velocity from the nozzle, results in a better control of drop size than in the isothermal problem; the evaporation time scale is assumed to be much longer than the viscous time scale here.

Lubrication theory has been used to investigate the dynamics of thin liquid sheets for nearly 40 years (see the reviews by Oron, Davis & Bankoff 1997 and Eggers 1997). The rupture of sheets and threads, in a lubrication theory context (see, for example, Erneux & Davis 1993), has been investigated in a variety of scenarios, including the use of surfactants (Craster, Matar & Papageorgiou 2002), electric fields (see Tilley, Petropoulus & Papageorgiou 2001, Savettaseranee *et al.* (2003), and Papageorgiou & Vanden-Broeck 2004), nematic liquid crystalline jets (see Cheong, Rey & Mather 2001), and van der Waals forces (Witelski & Bernoff (1999) and Vaynblat, Lister & Witelski 2001). In particular, Chwalek *et al.* (2002) used differential heating across a nozzle exit to induce bending of a jet from the nozzle at a prescribed angle. Brenner & Paruchuri (2003) then showed, through an equilibrium balance of net forces and torques, that the maximum deflection of this jet (or sheet) coincided with a Weber number of unity. The latter paper focused on altering the direction of the jet (or sheet), but not on the differences in the rupture dynamics.

2. Problem formulation

Consider a symmetric disturbance of a heated viscous sheet, as illustrated in figure 1. The equations that govern this system are the standard two-dimensional continuity

and Navier–Stokes equations coupled to a conservation of energy equation,

$$\nabla\cdot\boldsymbol{u}=0,\quad \boldsymbol{u}_t+\boldsymbol{u}\cdot\nabla\boldsymbol{u}=-\frac{1}{\rho}\nabla p+\nu\nabla^2\boldsymbol{u}, \tag{2.1}$$

$$T_t+\boldsymbol{u}\cdot\nabla T=\kappa\nabla^2 T. \tag{2.2}$$

Here, $\boldsymbol{u}=(u,w)$ is the fluid velocity, where u is the x-component and w is the z-component, ρ is the fluid density, ν is the fluid kinematic viscosity, p is the fluid pressure, T is the fluid temperature, and κ is the thermal diffusivity of the fluid.

As we are interested in symmetric disturbances, (2.1)–(2.2) are subject to the symmetry boundary conditions $u_z=w=T_z=0$ at $z=0$, corresponding to zero shear, vanishing vertical velocity and zero vertical temperature gradient, respectively, across the centre-line. Along the fluid interface $z=h(x,t)$, we require that the tangential stress is driven by gradients in surface tension

$$\frac{\mu}{1+h_x^2}\left\{(u_z+w_x)\left(1-h_x^2\right)-4u_xh_x\right\}=\nabla\sigma\cdot\boldsymbol{t}, \tag{2.3}$$

(where μ is the fluid dynamic viscosity) and that the normal stress is balanced by surface tension times the curvature

$$-p+\frac{2\mu}{1+h_x^2}\left\{u_x\left(h_x^2-1\right)-h_x(u_z+w_x)\right\}=\sigma\frac{h_{xx}}{\left(1+h_x^2\right)^{3/2}}. \tag{2.4}$$

The reduced surface tension σ is a consequence of the imposed temperature gradients, so that $\sigma=\sigma_0-\gamma(T-T_0)$, with γ being the rate at which surface tension depends linearly on temperature and where T_0 is the ambient temperature (corresponding to surface tension σ_0). The normal heat flux across the interface is given by Newton's law of cooling

$$k\nabla T\cdot\boldsymbol{n}=-H(T-T_0), \tag{2.5}$$

where k is the thermal conductivity and H is the heat transfer coefficient, while the standard kinematic condition is stated as

$$h_t+\frac{\partial}{\partial x}\int_0^h u\,\mathrm{d}z=0. \tag{2.6}$$

We non-dimensionalize our variables based on the following scales:

$$[x]=L,\quad [z]=h_0,\quad [u]=\frac{\nu}{h_0},\quad [w]=\frac{\nu}{L},\quad [t]=\frac{Lh_0}{\nu},\quad [p]=\frac{\rho\nu^2}{h_0^2},\quad T-T_0=\theta\Delta T,$$

where ΔT is a measure of the heating of the sheet. In terms of the non-dimensionalized variables, we find that

$$u_x+w_z=0, \tag{2.7}$$

$$\epsilon\{u_t+uu_x+wu_z\}=-\epsilon p_x+u_{zz}+\epsilon^2u_{xx}, \tag{2.8}$$

$$\epsilon^2\{w_t+uw_x+ww_z\}=-p_z+\epsilon\{w_{zz}+\epsilon^2w_{xx}\}, \tag{2.9}$$

$$\epsilon Pr\{\theta_t+u\theta_x+w\theta_z\}=\theta_{zz}+\epsilon^2\theta_{xx} \tag{2.10}$$

($\epsilon=h_0/L\ll 1$ is the aspect ratio and $Pr=\nu/\kappa$ is the Prandtl number). We also have

Dimensional scales

Parameter	Value
h_0 (cm)	10^{-3}
L (cm)	10^{-1}
ΔT (K)	10^{-2}–0.2
ρ (g cm^{-3})	1
ν (cm^2 s^{-1})	3×10^{-3}
μ (g cm^{-1} s^{-1})	3×10^{-3}
H (erg s^{-1} cm^{-2} K^{-1})	1×10^5
σ_0 (dyn cm^{-1})	60
γ (dyn cm^{-1} K^{-1})	0.2
k (erg cm^{-1} s^{-1} K^{-1})	7×10^4
κ (cm^2 s^{-1})	2×10^{-3}

Dimensionless quantities

Quantity	Value
ϵ	10^{-2}
M	0.2–4.44
B	0.143
S	0.667
Pr	1.5

TABLE 1. Parameter values for a water sheet in c. g. s. units and the non-dimensional equivalents.

$u_z = w = \theta_z = 0$ at $z = 0$ and free-surface boundary conditions:

$$(u_z + \epsilon^2 w_x)\left(1 - \epsilon^2 h_x^2\right) - 4\epsilon^2 u_x h_x = -\epsilon M\,(\theta_x + h_x \theta_z)\,\sqrt{1 + \epsilon^2 h_x^2}, \tag{2.11}$$

$$-p + \frac{2\epsilon}{1 + \epsilon^2 h_x^2}\left\{u_x\left(\epsilon^2 h_x^2 - 1\right) - h_x(u_z + \epsilon^2 w_x)\right\} = (S - \epsilon^2 M\theta)\,\frac{h_{xx}}{\left(1 + \epsilon^2 h_x^2\right)^{3/2}}, \tag{2.12}$$

$$\theta_z = -\epsilon B\theta\sqrt{1 + \epsilon^2 h_x^2} + \epsilon^2 \theta_x h_x, \tag{2.13}$$

$$h_t + \frac{\partial}{\partial x}\int_0^h u\,\mathrm{d}z = 0, \tag{2.14}$$

on the interface $z = h(x, t)$; $M = (\gamma \Delta T h_0)/(\mu\nu)$ is the Marangoni number, $S = (h_0^3 \sigma_0)/(\mu\nu L^2)$ is the capillary number and $B = (LH)/k$ is the Biot number.

In table 1 we show typical values of the physical parameters and their equivalent non-dimensional values (see also Burelbach, Bankoff & Davis 1988). The value of the Biot number corresponds to poor heat transport from the sheet to the surrounding environment compared to heat transport along the sheet. In addition, the Marangoni number M varies as a function of the initial heating of the fluid and, as indicated by table 1, can vary over the approximate range 0.2 to 4.44.

Expanding all of the dependent variables in powers of ϵ

$$u = u_0(x, z, t) + \epsilon u_1(x, z, t) + \cdots, \qquad w = w_0(x, z, t) + \epsilon w_1(x, z, t) + \cdots,$$
$$p = p_0(x, z, t) + \epsilon p_1(x, z, t) + \cdots, \qquad \theta = \theta_0(x, z, t) + \epsilon\theta_1(x, z, t) + \cdots,$$

and substituting into (2.7)–(2.10), yields, at leading order

$$u_{0zz} = 0, \quad p_{0z} = 0, \quad \theta_{0zz} = 0,$$

subject to the boundary conditions

$$z = 0 : \; u_{0z} = w_0 = \theta_{0z} = 0, \tag{2.15}$$

$$z = h : \; u_{0z} = \theta_{0z} = 0, \quad p_0 = -Sh_{xx}. \tag{2.16}$$

From this system of equations, we find that

$$u_0 = u_0(x, t), \quad p_0 = -Sh_{xx}, \quad w_0 = -u_{0x} z, \quad \theta_0 = \theta_0(x, t).$$

At $O(\epsilon)$, we find

$$w_{1z} = -u_{1x}, \quad u_{1zz} = p_{0x} + u_{0t} + u_0 u_{0x}, \quad p_{1z} = 0, \quad \theta_{1zz} = Pr\{\theta_{0t} + u_0\theta_{0x}\}, \quad (2.17a\text{–}d)$$

subject to the symmetry conditions $u_{1z} = w_1 = \theta_{1z} = 0$ at $z = 0$, along with the following interfacial conditions at $z = h(x, t)$:

$$u_{1z} = -M\theta_{0x}, \quad p_1 = -2u_{0x}, \quad \theta_{1z} = -B\theta_0. \quad (2.18a\text{–}c)$$

Integrating (2.17*a*) and (2.17*d*) from $z = 0$ to $z = h$ and using the stress conditions, (2.18*a*) and (2.18*c*), we find evolution equations which govern the leading-order axial velocity u_0 and the average temperature θ_0

$$u_{1z}\big|_0^h = -M\theta_{0x} = h\{u_{0t} + u_0 u_{0x} + Sh_{xxx}\},$$
$$\theta_{1z}\big|_0^h = -B\theta_0 = h\{Pr[\theta_{0t} + u_0\theta_{0x}]\}.$$

To close the system, we employ the kinematic condition (2.14) and so obtain the following coupled equations for u_0, θ_0 and h:

$$u_{0t} + u_0 u_{0x} = Sh_{xxx} - M\frac{\theta_{0x}}{h}, \quad (2.19)$$

$$Pr\{\theta_{0t} + u_0\theta_{0x}\} = -\frac{B\theta_0}{h}, \quad (2.20)$$

$$h_t + \{u_0 h\}_x = 0. \quad (2.21)$$

In the isothermal situation, this system reduces to the system found by Matsuuchi (1974, 1976), Pugh & Shelly (1998), and Mehring & Sirignano (1999). This system yields quasi-periodic solutions for initial velocities below a critical value, but exhibits finite-time singularities (due to a balance of inertial effects and surface tension effects) when inertial effects are significant.

3. Results

In investigating the system (2.19)–(2.21) (we drop the zero subscripts in the following for notational clarity), we restrict ourselves to spatially periodic boundary conditions on the domain $0 \leqslant x \leqslant 2\pi$. The typical mechanism to drive a cylindrical jet to rupture in ink-jet printing applications is by modulation of the pressure near the nozzle exit. We analogously model this phenomenon for a sheet by looking at an initial sinusoidal variation of the axial velocity, $u(x, 0) = U_0 \sin k_u x$, where U_0 is the velocity resulting from this pressure disturbance (or equivalently the Reynolds number of the flow) and k_u is the wavenumber of the velocity disturbance. Under typical operating conditions of ink-jet printers, $U_0 \approx 10$. This magnitude reflects the desire to produce drops quickly (short times to rupture), and not the minimum velocity magnitude at which rupture can occur. For the isothermal version of (2.19)–(2.21), $U_0 \approx 0.85$ is the minimum value for which rupture in this system can occur (see Tilley *et al.* 2001). We are interested in how initial heating of the sheet affects the transient dynamics toward rupture.

We also assume there to be an initial temperature distribution across the sheet,

$$\theta(x, z, 0) = \sin k_\theta x,$$

which is induced after a period of localized heating; at leading order, we find no z-variation in θ. The wavenumber of the temperature disturbance is denoted by k_θ. Note that since we scaled temperature on the initial difference between maximum heating and ambient, this initial condition has unit amplitude. In this sense, the

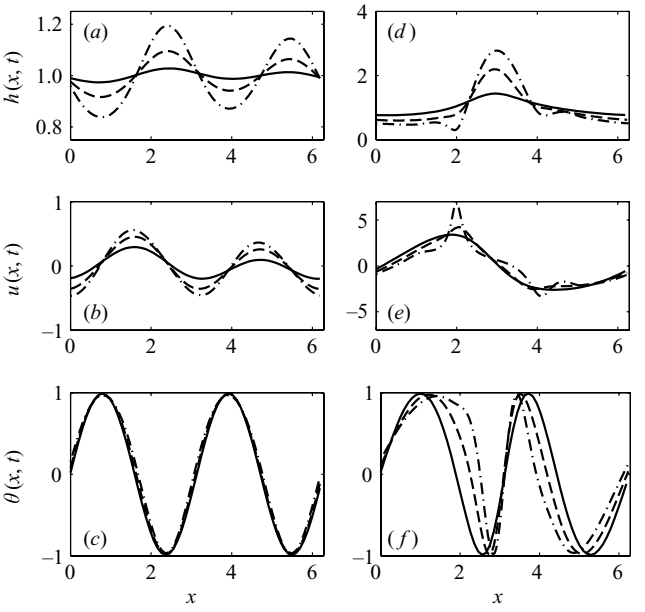

FIGURE 2. The initial transients at times $t = 0.1$ (solid curve), $t = 0.2$ (dashed curve) and $t = 0.3$ (dashed-dot curve) with $M = S = Pr = 1$: (a) interfacial deflection, (b) axial velocity, (c) temperature for $U_0 = 0.1$; and (d–f) as (a–c) but for $U_0 = 3$. For $U_0 = 0.1$, fluid inertia plays a minor role. Within $t = 0.1$, Marangoni stresses have induced a flow with wavenumber $k = 2$, and the initial interfacial deflection results in a slightly sharper velocity gradient near the first peak of the initial temperature distribution $x = x_1$. For $U_0 = 3$, inertia plays a significant role. Marangoni stresses weakly drain the film at the desired location, allowing for a control of the rupture location. Advection of heat, however, counteracts this control mechanism.

Marangoni number M provides a measure of the initial heating. In addition, we assume for simplicity that the initial interfacial condition is given by $h(x, 0) = 1$. This variable is the most difficult to control in applications. Finally, we note that the characteristic rupture time scale is significantly shorter than the time scale corresponding to thermal losses.

We investigate the solutions to (2.19)–(2.21) numerically by use of a pseudo-spectral expansion in space and a Runge–Kutta method in time (see Tilley *et al.* 2001 and Savettaseranee *et al.* 2003). The time step is adaptive and depends on the number of spatial modes whose amplitudes are greater than some prescribed tolerance, typically between 10^{-10} and 10^{-12}. Furthermore, the solution is spectrally interpolated when $N/2 - 5$ modes have an amplitude larger than this prescribed criterion (where N is the number of collocation points). The numerical solution is terminated when the minimum interfacial height is below 1% of its initial value.

We begin by considering the possible control mechanisms. In figure 2(a–c), we show the initial transient for the parameter values $M = 1$, $U_0 = 0.1$, $k_\theta = 2$ and $k_u = 1$. The initial temperature distribution induces a flow through surface-tension gradients, resulting in the largest velocity gradients near $x_1 = \pi/2$ and $x_2 = 3\pi/2$. The film drains most rapidly near these regions. However, the initial velocity distribution leads to a slightly sharper velocity gradient near $x = x_1$ compared to that near $x = x_2$, resulting in a quicker rate of draining near $x = x_1$. Since the sheet will be thinner near $x = x_1$ compared to $x = x_2$ during these times, this results in rupture occurring first near $x = x_1$. This example is illustrative of a situation where Marangoni effects play a

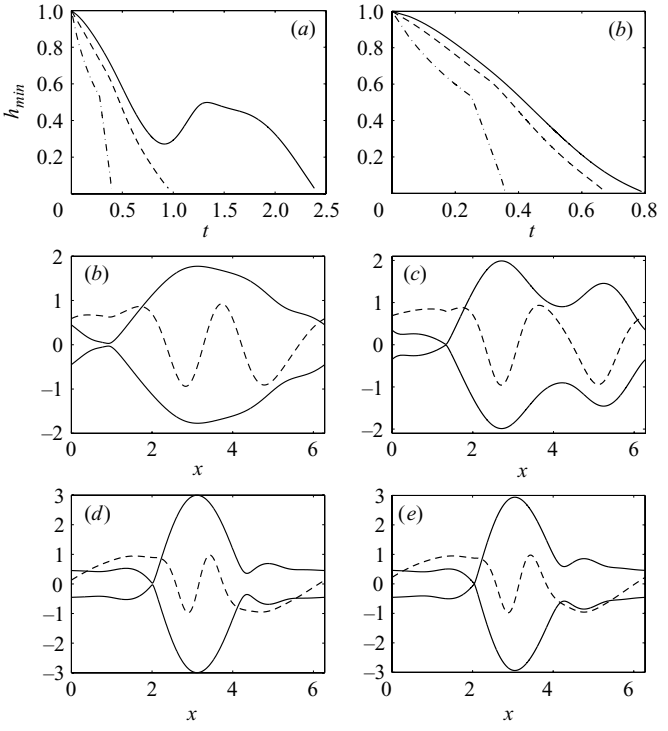

FIGURE 3. (*a*) Evolution of the minimum interfacial height, h_{min}, when $M = 1$, for $U_0 = 0.4$ (solid curve), $U_0 = 1$ (dashed curve), and $U_0 = 3$ (dash-dot curve). The corresponding final distribution of the interfacial shape (solid curve) and the temperature profile (dashed curve) are shown for (*b*) $U_0 = 1$ and (*c*) $U_0 = 3$. (*d–f*) The analogous $M = 2$ case.

dominant role. The Marangoni stresses act to increase the local velocity gradients and these gradients then drain the film at the desired location, providing control of film rupture. When $U_0 = 3$, the potential rupture location is determined by inertial effects. As figures 2(*d–f*) show, the sheet tends to rupture quickly by the interaction of inertia and surface tension forces. Marangoni effects in this case are not strong enough to modify the dynamics significantly, and the rupture location, $x_r \approx 1.95$, is not local to either x_1 or x_2.

In figure 3(*a*) (where we have taken $M = 1$), we plot the minimum interfacial height as a function of time for $U_0 = 0.4$, 1, and 3. The final interfacial shape (solid curve) and the temperature distribution (dashed curve) for $U_0 = 1$ and 3 are shown as figures 3(*b*) and 3(*c*) respectively. Figure 3(*d–f*) shows the corresponding $M = 2$ case. Increasing the Marangoni number M significantly reduces the time taken for rupture to occur. Notice that the potential drop size can be controlled with a combination of the initial temperature distribution and the strength of the initial axial velocity disturbance.

In figure 4(*a*) we show the final minimum interfacial location x_{min} as a function of M for $U_0 = 1$ and $M = 0.1$–1. Figure 4(*b*) shows the corresponding minimum interfacial height. Note that there is a distinct pattern of rupture that occurs for the smaller values of the Marangoni number compared to the larger values. For smaller Marangoni numbers, the minimum interfacial height is localized near $x_{min} \approx 0.6$ until near the rupture time, where a second minimum near $x_{min} \approx 6$ goes to rupture. For larger values of the Marangoni number, the original minimum results in the rupture

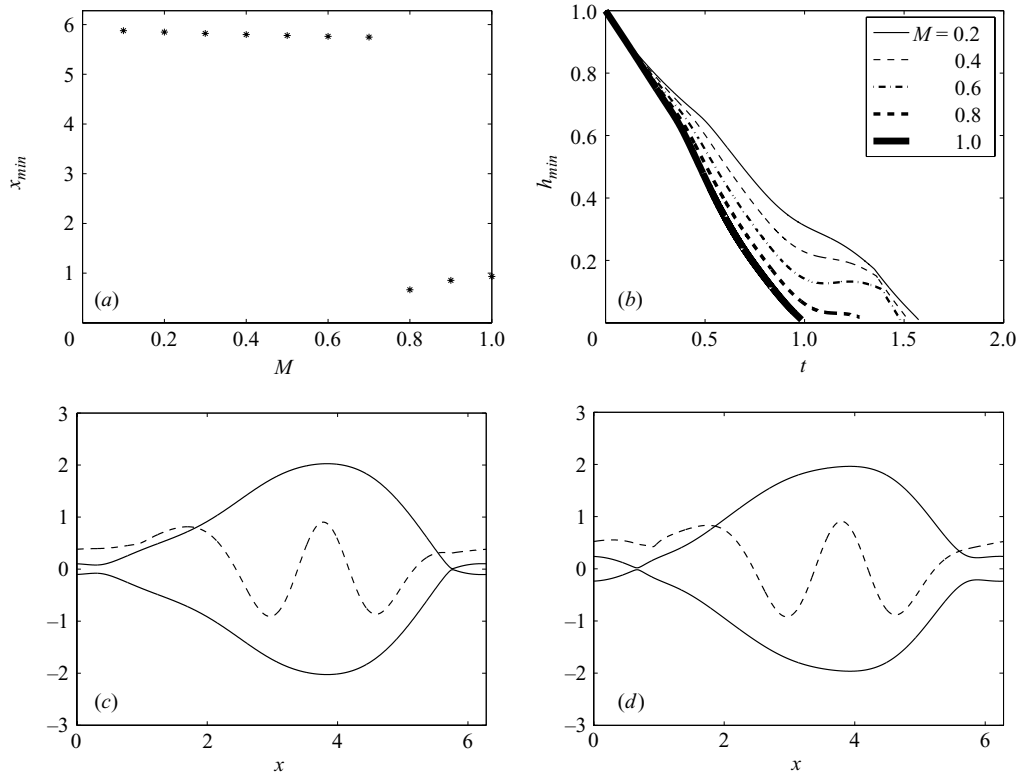

FIGURE 4. (*a*) Minimum interfacial height location, and (*b*) the minimum interfacial height versus time for Marangoni numbers $M = 0.1$–1 with $U_0 = 1$. Intermediate values of the Marangoni number lead to a transition in the rupture location from near $x = 0.6$ to near $x = 6$. (*c*) Final interfacial distribution (solid curve) and temperature distribution (dashed curve) for $M = 0.6$. (*d*) As (*c*) but for $M = 0.8$.

location. Figures 4(*c*) and 4(*d*) show the final wave profiles for $M = 0.6$ and 0.8, respectively.

One measure of how sensitive the location of the rupture point is to variations in the axial velocity field is to assume a phase difference between the initial conditions in u and θ. In figures 5(*a*) (where $M = 1$) and 5(*b*) (where $M = 2$), we show the results of several simulations for $u(x, 0) = U_0 \sin(x + \phi)$ (with $U_0 = 1$) and $\theta(x, 0) = \sin(2x)$. In figure 5(*a*), we notice that rupture can occur (or not occur) by even slight differences in phase. In this case, initial inertial stresses dominate the Marangoni forces. However, by a judicious choice of the phase shift, the two effects can work in collaboration to minimize the rupture time. For larger values of M, the phase difference does not affect the time of rupture as significantly, but it does offer a secondary mechanism to control the rupture location (as can be seen in figure 5*b*).

4. Conclusions

We have considered quantitatively how a weak localized heating of a thin fluid sheet could be used to control the location of, and time to, rupture. A lubrication approximation takes account of changes in the sheet thickness, axial velocity, and average temperature. Viscous effects are neglible in this particular case. The resulting

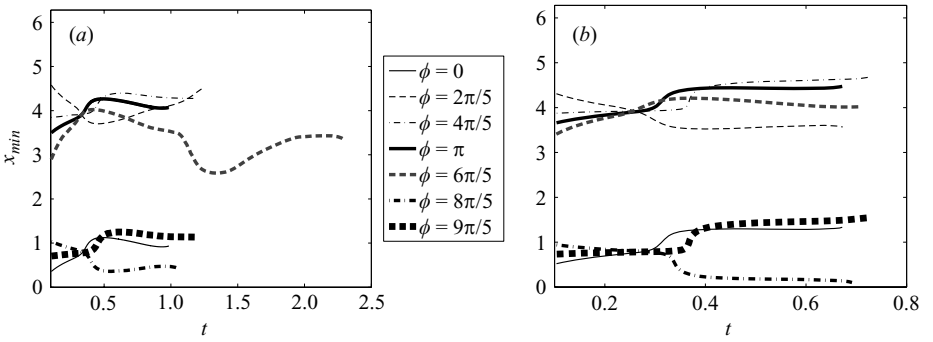

FIGURE 5. The location of the minimum interfacial location x_{min} over time (for the case when $U_0 = 1$) for different phase shifts ϕ between the initial velocity field $u(x, 0)$ and the initial temperature field $\theta(x, 0)$. In each case, the simulation is terminated when the rupture criterion of $h_{min} = 0.01$ is reached. (*a*) $M = 1$ and (*b*) $M = 2$; note that the phase shift at this value of M results in a relatively clean distinction of the rupture location x_{min} and comparable rupture times.

system is nearly conservative due to the poor heat transport from the sheet to the surrounding environment. From this study, we have found that when the Marangoni stresses are comparable to inertial effects, then there is some control of the rupture point and time. However, the lack of significant dissipative mechanisms makes controlling some aspects of the rupture challenging. If more dissipation can be introduced into the system (or equivalently if surface tension effects were comparable to viscous effects), then the mechanism for control would be improved, but at a cost on the rupture time scale.

Furthermore, a reduction of the rupture time is dependent upon the difference in phase between the initial axial velocity and the initial temperature profile. To extend this analysis to include larger Marangoni stresses requires an understanding of pressure variations in the surrounding environment. We are currently investigating this scenario in cylindrical geometries, where the instability is driven primarily by the hoop-stress terms due to surface tension.

We would like to thank the Banff International Research Station where our collaboration originated, and M. B. gratefully acknowledges the support of an EPSRC Postdoctoral Fellowship.

REFERENCES

BRENNER, M. & PARUCHURI, S. 2003 Thermal bending of liquid sheets and jets. *Phys. Fluids* **15**, 3568.

BURELBACH, J., BANKOFF, S. & DAVIS, S. 1988 Nonlinear stability of evaporating/condensing liquid films. *J. Fluid Mech.* **195**, 463–494.

CHEONG, A.-G., REY, A. & MATHER, P. 2001 Capillary instabilities in thin nematic liquid crystalline fibers. *Phys. Rev.* E **64**, 041701.

CHWALEK, J., TRAUERNICHT, D., DELAMETTER, C., SHARMA, R., JEANMAIRE, D., ANAGOSTOPOULOS, C., HAWKINS, G., AMBRAVANESWARAN, B., PANDITARATNE, J. & BASARAN, O. 2002 A new method for deflecting liquid microjets. *Phys. Fluids* **14**, L37.

CRASTER, R., MATAR, O. & PAPAGEORGIOU, D. 2002 Pinchoff and satellite formation in surfactant covered viscous threads. *Phys. Fluids* **14**(4), 1364.

EGGERS, J. 1997 Nonlinear dynamics and breakup of free-surface flows. *Rev. Mod. Phys.* **69**, 865.

ERNEUX, T. & DAVIS, S. 1993 Nonlinear rupture of free films. *Phys. Fluids* A **5**, 1117.

Garnier, N., Grigoriev, R. & Schatz, M. 2003 Optical manipulation of microscale fluid flow. *Phys. Rev. Lett.* **91**, 054501.

Hayes, D., Wallace, D. & Cox, W. R. 1999 Microjet printing of solder and polymers for multi-chip modules and chip-scale packages. *Proc. SPIE* vol. 3830, 242.

Matsuuchi, K. 1974 Modulational instability of nonlinear capillary waves on thin liquid films. *J. Phys. Soc. Japan* **37**, 1680.

Matsuuchi, K. 1976 Instability of thin liquid sheet and its break-up. *J. Phys. Soc. Japan* **41**, 1410.

Mehring, C. & Sirignano, W. 1999 Nonlinear capillary wave distortion and disintegration of thin planar liquid sheets. *J. Fluid Mech.* **388**, 69.

Molesa, S., Redinger, D., Huang, D. & Subramanian, V. 2003 High-quality inkjet-printed multilevel interconnects and inductive components on plastic for ultra-low-cost RFID applications. *Mat. Res. Soc. Symp. Proc.* 769.

Nahas, N. & Panton, R. 1990 Control of surface tension flows: Instability of a liquid jet. *Trans. ASME: J. Fluids Engng* **112**, 296.

Oron, A., Davis, S. & Bankoff, S. 1997 Long-scale evolution of thin liquid films. *Rev. Mod. Phys.* **69**, 931.

Papageorgiou, D. & Vanden-Broeck, J.-M. 2004 Large amplitude capillary waves in electrified fluid sheets. *J. Fluid Mech.* **508**, 71.

Pugh, M. & Shelley, M. 1998 Singularity formation in thin jets with surface tension. *Commun. Pure Appl. Maths* **51**, 733.

Rybalko, S., Magome, N. & Yoshikawa, K. 2004 Forward and backward laser-guided motion of an oil droplet. *Phys. Rev.* E **70**, 046301.

Savettaseranee, K., Papageorgiou, D., Petropoulos, P. & Tilley, B. 2003 The effect of electric fields on the rupture of thin viscous films by van der Waals forces. *Phys. Fluids* **15**, 641.

Schatz, M. & Neitzel, G. 2001 Experiments on thermocapillary instabilities. *Annu. Rev. Fluid Mech.* **33**, 93.

Sumner, L., Wood, A. & Neitzel, G. 2003 Lubrication analysis of thermocapillary-induced nonwetting. *Phys. Fluids* **15**, 2923.

Tilley, B., Petropoulos, P. & Papageorgiou, D. 2001 Dynamics and rupture of planar electrified liquid sheets. *Phys. Fluids* **13**, 3547.

Vaynblat, D., Lister, J. & Witelski, T. 2001 Rupture of thin films by van der Waals forces: Evolution and self-similarity. *Phys. Fluids* **13**, 1130.

Witelski, T. & Bernoff, A. 1999 Stability of self-similarity solutions for van der Waals driven thin film rupture. *Phys. Fluids* **11**, 2443.